^{13}C Double-Resonance Fourier-Transform Spectroscopy in Solids*

P. K. Grannell† and P. Mansfield
Department of Physics, University of Nottingham, Nottingham, England

M. A. B. Whitaker
School of Physical Sciences, New University of Ulster, Coleraine, Co. Londonderry, Northern Ireland

(Received 12 April 1973)

A high-resolution double-resonance scheme is described which enables measurements of the chemical-shift structure and intrinsic line shape in low-abundance spin species in solids. Expressions for the decay function and the line-shape function are formulated. As a theoretical test of the range of validity of the scheme, simulated signal decays and line shapes are regenerated using a Gaussian-decay input function and fixed parameters covering a range common to ^{13}C in natural abundance. As examples of its application the method is used to study the 1.108% naturally abundant ^{13}C in a number of organic solids. The preliminary results presented are encouraging and indicate the presence of chemical-shift splittings and anisotropies.

I. INTRODUCTION

In the pulsed nuclear-double-resonance technique of Hartmann and Hahn[1] and the later modification of Lurie and Slichter,[2] dilute spins in a solid can be observed indirectly through their effect on a second high-natural-abundance spin species. In both schemes, however, the effective resolution of the rare-spin system is poor since the width of the double-resonance destruction line shape is dominated by the spin-spin interaction of the abundant species.[1] For organic solids where the double resonance may be between the 100%-abundant protons or fluorine nuclei and the 1.108%-abundant ^{13}C spins, the observed destruction spectrum corresponds to a sensitivity enhancement of about 10^4 and is typically of the order of 50 kHz in width. The width may be reduced by a factor of 3 or so by performing the abundant-species spin locking in the tilted rotating reference frame[3] at the magic angle $\theta = \cos^{-1}(1/\sqrt{3})$. The price paid for this line narrowing is a slow down of the rate at which the abundant spins and hence the whole spin system approaches thermodynamic equilibrium. In terms of high resolution, the gains are small.

In spite of the relatively poor resolution, the original double-resonance schemes and variations involving field cycling have been used with considerable success in the study of dilute spins or even just weak resonances.[4–20] In most of these instances the linewidth of the dilute spin system is broadened by a quadrupole interaction which is often much larger than the dipolar interaction of the abundant species.

The double-resonance technique has also formed the vehicle for experimental and theoretical studies of the spin dynamics of cross-relaxation and multiple quantum transitions in the doubly rotating reference frame.[21–26]

In order to improve the resolution of the double-resonance technique, so that dilute-spin line shapes, which include chemical shifts and their anisotropies, could be studied, we recently proposed[27,28] modifications to the Lurie-Slichter scheme,[2] pointing out the usefulness of our technique for the study of dilute spin systems with small quadrupole splittings, resonances of isolated groups of spins, for example, dilute methyl groups, etc. Since our first paper,[27] a number of papers have appeared on the subject of high-resolution double resonance in solids, using slightly different double-resonance techniques.[29–35]

As far as we can tell, the resolution in the Bleich-Redfield method will depend on such factors as rf inhomogeneity and residual heteronuclear dipolar interactions. The experiment of Pines *et al.*[31] is itself a variant of the original Lurie-Slichter method of pulsed double resonance, where in this case the rare spins, rather than the abundant-spin system, are observed directly, signal averaged, and finally Fourier transformed in a computer. As with our experiment, the rare spins undergo free precession in the static magnetic field, so making this method capable of achieving high resolution. In both our method and that of Pines *et al.*, the resolution limitations will be static-field inhomogeneity and the degree to which the heteronuclear dipolar interaction is stirred out by the abundant-species spin-locking rf field.[36]

In this paper we present a detailed analysis of our method for high-resolution double-resonance studies of dilute spin systems in solids. In Sec. III the expressions derived are evaluated numerically in order to assess the fidelity of line shapes produced experimentally. A brief discussion of sensitivity is given in Sec. IV. Experimental tests of the method are described in Sec. V and preliminary results of the application of the technique

are given for the measurements of ^{13}C chemical shifts in some compounds.

II. HIGH-RESOLUTION DOUBLE-RESONANCE METHOD

A. Description

In the Lurie-Slichter method of pulsed double resonance, the abundant I spin system is spin locked at exact resonance, while the rare-S-spin system is simultaneously irradiated with a train of coherent rf pulses close to its Larmor frequency ω_{0S}. Thermal mixing of the two spin systems occurs via cross relaxation when both rf fields are on. The combined system approaches thermodynamic equilibrium, characterized by a common spin temperature. The S-channel rf field is turned off for a period τ, greater than the spin-spin interaction time of the rare-spin system T_{2S}, thus allowing the dilute system to approach an infinite spin temperature.

In an important variation of this method, with which our technique is closely related, McArthur *et al.*[37] showed that the rare-spin free-induction-decay (FID) function on resonance $G(\tau)$ could be mapped out by varying τ from zero to a few times T_{2S}. Indeed, the linewidth of the 0.13%-abundant ^{43}Ca in calcium fluoride was measured in this way.[37] However, they failed to realize that the method would work with the S spins off resonance, an important point, as we shall see, when considering asymmetric line shapes. Furthermore, since the I spins were adiabatically demagnetized in the rotating frame, the heteronuclear dipolar interaction was not stirred out.

In our technique, we exploit the fact that the S spins may be off resonance. The procedure follows closely the Lurie-Slichter scheme described above, except that the time between thermal contacts is, in general, of the order of T_{2S} so that some S-spin transverse magnetization remains. If its precession frequency differs from that of the S-channel rf-field carrier frequency, the S magnetization can reverse its direction with respect to that of the rf field. Thus on restoring the rf field, positive or negative S-spin temperatures may be created. Since a negative S-spin temperature is more effective at destroying the I magnetization, as we shall see later, this leads for many thermal mixing pulses of fixed τ to an amplitude modulation of the I-spin destruction spectrum as a function of frequency.

B. Theory

1. Fixed t and τ

Consider the I-spin system which is spin locked in the rotating frame at exact resonance ω_{0I} along an rf magnetic field of amplitude H_{1I}. The S spins are simultaneously irradiated by a train of N pulses of rf magnetic field with amplitude H_{1S} and at angular frequency ω_S close to their Larmor angular frequency ω_{0S}. Each pulse has a duration t, and the off time between pulses is τ.

During the Nth thermal contact pulse, the approach to equilibrium of the I magnetization is given by[38]

$$M_{IN}(t)=[M_{IN}(0)-M_{IN}(\infty)]e^{-t/T_{CR}}+M_{IN}(\infty), \qquad (1)$$

where $M_{IN}(t)$ is the I magnetization at a time t after the beginning of the Nth thermal contact, and $M_{IN}(0)$ is the initial magnetization. This is, of course, equal to the magnetization remaining at the end of the previous thermal contact; i.e.,

$$M_{IN}(0)=M_{I(N-1)}\,. \qquad (1a)$$

We assume that the cross-relaxation process may be described by a single exponential function with a characteristic time constant T_{CR}. Except for very short times t, this is a good approximation.[4,22,37]

The growth of the S magnetization during the Nth thermal contact is given by an equation of similar form

$$M_{SN}(t)=[M_{SN}(0)-M_{SN}(\infty)]e^{-t/T_{CR}}+M_{SN}(\infty). \qquad (2)$$

Since the S magnetization is allowed to freely precess in the off time τ, between the $(N-1)$th and Nth thermal contact pulses, the initial S magnetization at $t=0$ is related to the previous magnetization by

$$M_{SN}(0)=M_{S(N-1)}(t)\,\Gamma(\tau), \qquad (2a)$$

where $\Gamma(\tau)$ is the S-spin FID function.

The equilibrium spin magnetization is given, in general, by the Curie law[2]

$$\vec{M}=C\vec{H}/\Theta, \qquad (3)$$

where Θ is the equilibrium spin temperature and Curie's constant $C=N_I\gamma_I^2\hbar^2I(I+1)/3k$. N_I in this expression is the number of spins. The other terms have their usual meanings.

The magnetic energy of a spin system is given by

$$E=-\vec{M}\cdot\vec{H}=-CH^2/\Theta\,. \qquad (4)$$

Equating the magnetic energy of the combined spin system at the beginning to that at the end of the Nth thermal contact pulse, we get for complete cross relaxation to a common spin temperature $\Theta_{fN}(\infty)$, using Eqs. (3) and (4),

$$\frac{1}{\Theta_{I(N-1)}}+\frac{\epsilon\Gamma(\tau)}{\Theta_{S(N-1)}}=\frac{1+\epsilon}{\Theta_{fN}(\infty)}\,, \qquad (5)$$

where $\Theta_{fN}(\infty)=\Theta_{IN}(\infty)=\Theta_{SN}(\infty)$. The quantity ϵ is defined as

$$\epsilon=C_S H_{1S}^2/C_I\,(H_{1I}^2+H_L^2), \qquad (6)$$

in which the local field H_L is given by[2]

$$H_L^2 = \tfrac{1}{3}M_{2II} + M_{2IS} + \frac{\gamma_S^2 N_S S(S+1)}{3\gamma_I^2 N_I I(I+1)} M_{2SS} . \quad (7)$$

Here M_{2II} and M_{2SS} are the Van Vleck second moments[39] of the I spins alone and the S spins alone, respectively, and M_{2IS} is the S-spin contribution to the second moment of the I spins. Substituting for $\Theta_{IN}(\infty)$ from Eq. (5) above into Eqs. (3) and (1) gives

$$M_{IN}(t) = M_{I(N-1)}\left(\frac{1+\epsilon e^{-t/T_{CR}}}{1+\epsilon}\right) + M_{S(N-1)}\left(\frac{C_I H_{1I}}{C_S H_{1S}}\right)\left(\frac{1-e^{-t/T_{CR}}}{1+\epsilon}\right)\epsilon\Gamma(\tau). \quad (8)$$

Similarly, Eqs. (2), (3), and (5) give

$$M_{SN}(t) = M_{S(N-1)}\,\Gamma(\tau)\left(\frac{\epsilon+e^{-t/T_{CR}}}{1+\epsilon}\right) + M_{I(N-1)}\left(\frac{C_S H_{1S}}{C_I H_{1I}}\right)\left(\frac{1-e^{-t/T_{CR}}}{1+\epsilon}\right). \quad (9)$$

If $H_{1I}^2 \gg H_L^2$ so that $\epsilon \simeq C_S H_{1S}^2/C_I H_{1I}^2$, and writing $\eta = H_{1I}/H_{1S}$, we may write the coupled equations (8) and (9) in matrix form as

$$\begin{pmatrix} M_{IN} \\ M_{SN}/\eta \end{pmatrix} = \begin{bmatrix} a & b \\ d & c \end{bmatrix} \begin{pmatrix} M_{I(N-1)} \\ M_{S(N-1)}/\eta \end{pmatrix}, \quad (10a)$$

where

$$a = (1+\epsilon e^{-t/T_{CR}})/(1+\epsilon), \quad (10b)$$

$$b = \Gamma(\tau)(1-e^{-t/T_{CR}})/(1+\epsilon), \quad (10c)$$

$$c = \Gamma(\tau)(\epsilon+e^{-t/T_{CR}})/(1+\epsilon), \quad (10d)$$

$$d = \epsilon(1-e^{-t/T_{CR}})/(1+\epsilon). \quad (10e)$$

At the start of the first thermal contact, $M_{S(0)} = 0$ and $M_{I(0)} = C_I H_0/\theta_L = M_{0I}$ (the initial spin-locked I magnetization[1]), where θ_L is the lattice temperature, and H_0 the static magnetic field strength. Substituting these initial conditions into Eq. (10a) gives

$$\begin{pmatrix} M_{IN} \\ M_{SN}/\eta \end{pmatrix} = \underline{A}^N \begin{pmatrix} 1 \\ 0 \end{pmatrix} M_{0I}, \quad (11)$$

where

$$\underline{A}^N = \begin{bmatrix} a & b \\ d & c \end{bmatrix}.$$

This matrix equation may be solved for M_{IN}/M_{0I} explicitly by diagonalizing $\underline{A}$ and we shall resort to this method later when describing more complicated experiments. A somewhat simpler method is the following. We seek a solution to Eq. (11) such that

$$fM_{IN} + M_{SN}/\eta = k(fM_{I(N-1)} + M_{S(N-1)}/\eta); \quad (12)$$

substituting for M_{IN} and M_{SN}/η from Eq. (11) into Eq. (12) and equating coefficients of $M_{I(N-1)}$ and $M_{S(N-1)}/\eta$ gives

$$fa + d = kf \quad (13a)$$

and

$$fb + c = k, \quad (13b)$$

whence

$$f_\pm = (a-c)/2b \pm (1/2b)[(a-c)^2 + 4bd]^{1/2} \quad (14)$$

and

$$k_\pm = \tfrac{1}{2}(a+c) \pm \tfrac{1}{2}[(a+c)^2 - 4(ac-bd)]^{1/2}. \quad (15)$$

By invoking the initial conditions and iterating Eq. (12) N times, we obtain

$$f_\pm M_{IN} + M_{SN}/\eta = k_\pm^N f_\pm M_{0I}, \quad (16)$$

which yields directly

$$\frac{M_{IN}}{M_{0I}} = \frac{f_+ k_+^N - f_- k_-^N}{f_+ - f_-} = \frac{M(N)}{M(0)}, \quad (17)$$

where we have simplified our notation slightly.

The I- and S-spin rotating-frame spin-lattice relaxation times are here assumed to be infinite. Spin-lattice relaxation effects may be accounted for phenomenologically in the coupled relaxation equations, the general forms of which are given by Whitaker and Mansfield[38] for a single thermal mixing interaction.

2. *Approximations*

Equation (17) is completely general within the assumptions made in its derivation. However, it is useful to consider the solution in special cases. It is easy to show from Eq. (10) that

$$ac - bd = \Gamma(\tau)e^{-t/T_{CR}}. \quad (18)$$

If $\Gamma(\tau)e^{-t/T_{CR}} = 0$, then Eq. (17) reduces to

$$\frac{M(N)}{M(0)} = \frac{1+\epsilon e^{-t/T_{CR}}}{1+\epsilon}\left(\frac{1+\epsilon[\Gamma(\tau)+e^{-t/T_{CR}}]}{1+\epsilon}\right)^N, \quad (19)$$

valid for any ϵ and N. If we now take $\epsilon \ll 1$, Eq. (19) further simplifies to

$$M(N)/M(0) = [1-\epsilon\Gamma(\tau)] \times \exp\{-N\epsilon[1-\Gamma(\tau)-e^{-t/T_{CR}}]\}. \quad (20)$$

If, on the one hand, $\Gamma(\tau) = 0$, Eq. (20) reduces to the result of Lurie and Slichter[2] and Lang and Moran.[22] On the other hand, if $t \gg T_{CR}$ it reduces essentially to the result of McArthur *et al.*[37] if $\Gamma(\tau)$ is a monotonic decay function.

3. *Destruction-Spectrum Modulation*

The S-spin normalized free-induction decay for a line broadened by both homogeneous and inhomo-

geneous terms may be written

$$\Gamma(\tau)=\sum_i a_i G_i(\tau)\cos(\Delta\omega+\delta_i)\tau, \tag{21}$$

where a_i is the fraction of the S spins which have a resonance shift δ_i and a homogeneous decay function $G_i(\tau)$, and small S-channel angular frequency shifts are denoted $\Delta\omega=\omega_{0S}-\omega_S$. The above expression is, of course true only if the I spins are vigorously stirred with the I-channel spin-locking rf field.[36] In this case the effect of the heteronuclear dipolar interaction is averaged to zero.

If $t\gg T_{CR}$, substitution of Eq. (21) into Eq. (20) indicates a variation of magnetization with $\Delta\omega$ for fixed τ. For chemically equivalent spins, Eq. (20) predicts a cosine modulation of $\ln[M(N)/M(0)]$ with angular frequency $\Delta\omega$. This modulation of the destruction spectrum permits higher resolution of the resonance center of the rare spins, since the width of the central modulation peak for $\Delta\omega\sim 0$ is clearly of the order of $1/\pi\tau$. In practice the modulation amplitude decreases for longer τ through the $G(\tau)$ dependence, so that as one might expect, resolution is in fact limited by the approximate condition $\Delta\omega_{\min}\sim 1/T_{2S}^{*}$, where T_{2S}^{*} is the spin-spin interaction time of the S spins, which includes static-field inhomogeneity effects.

A complication arises if the S spins have a distribution of resonance shifts δ_i resulting in an asymmetric absorption line shape $\Gamma''(\Delta\omega)$. In this case the FID function $\Gamma(\tau)$ will comprise two signal components in quadrature and is represented on resonance by the complex decay function

$$\Gamma(\tau)=x(\tau)+iy(\tau) \tag{22}$$

and off resonance by the function

$$\Gamma(\tau,\Delta\omega)=[x(\tau)+iy(\tau)]e^{i\Delta\omega\tau}. \tag{23}$$

Since the experiment detects only that component of $\Gamma(\tau,\Delta\omega)$ which is along H_{1S}, the central modulation peak occurs at that angular frequency ω'_{0S} for which the real part of the FID is a maximum; that is to say, when

$$\frac{d}{d(\Delta\omega)}\,\mathrm{Re}[\Gamma(\tau)e^{i\Delta\omega\tau}]=0. \tag{24}$$

which leads to

$$\Delta\omega'_{0S}=\omega_{0S}-\omega'_{0S}=\frac{1}{\tau}\tan^{-1}\left(\frac{-y(\tau)}{x(\tau)}\right). \tag{25}$$

The function $\Gamma(\tau)$ may be represented by an expansion of the line-shape moments

$$\Gamma(\tau)=\sum_n M_n(i\tau)^n/n!, \tag{26}$$

in which the odd moments are retained. If the correct resonance frequency is taken to be the spectral point about which the first moment vanishes, then for small τ, substitution of Eq. (26) into Eq. (25) yields

$$\Delta\omega'_{0S}\simeq-\tfrac{1}{6}M_3\tau^2. \tag{27}$$

Thus the apparent resonance frequency of the S spins varies with τ, though the true resonance frequency may be found in the limit $\tau\to 0$. Of course, if $\Gamma''(\Delta\omega)$ is symmetric about ω_{0S}, then all odd moments vanish, $\Gamma(\tau)$ is real, and $\Delta\omega'_{0S}=0$ for all τ.

C. Fourier-Transform Spectroscopy

If the S-spin rf frequency ω_S is held constant while τ is varied in a series of separate experiments from near zero to values around several times T_{2S}, Eq. (20) shows that the residual I magnetization maps out the S-spin free-induction decay $\Gamma(\tau)$. Rearranging this equation and neglecting $\epsilon\Gamma(\tau)$ gives for $t\ll T_{CR}$,

$$\Gamma(\tau)=\{\ln[M(N)/M(0)]\}/N\epsilon+1. \tag{28}$$

The decay function $\Gamma(\tau)$ is related to the complex susceptibility $\Gamma(\Delta\omega)$ by the Fourier integral,[40-42]

$$\Gamma(\tau)=\int_{-\infty}^{\infty}\Gamma(\Delta\omega)e^{-i\Delta\omega\tau}d(\Delta\omega), \tag{29}$$

where for an inhomogeneously broadened line shape, with no dipolar broadening,

$$\Gamma(\Delta\omega)=K\sum_i a_i[-i\pi\delta(\Delta\omega+\delta_i)+\mathcal{P}(1/(\Delta\omega+\delta_i))]. \tag{30}$$

In this expression a_i is the fraction of the S spins with resonance shift δ_i, $\mathcal{P}$ denotes the Cauchy principal part of the integral, and

$$K=-\gamma_S\omega_{0S}N_S S(S+1)/3k\Theta_L. \tag{30a}$$

All other symbols have their usual meanings. Integration of Eq. (29) gives

$$\Gamma(\tau)=K\sum_i a_i(\cos\delta_i\tau-i\sin\delta_i\tau)$$
$$=x(\tau)+iy(\tau) \tag{31}$$

for $\tau\geq 0$, and $\Gamma(\tau)=0$ for $\tau<0$. For an asymmetric distribution of resonance shifts, the summation of sine terms does not vanish. So, when regenerating the absorption line shape from the free-induction decay, both the real and imaginary components must be included in the full Fourier transform,

$$\Gamma''(\Delta\omega)=\int_{-\infty}^{\infty}[x(\tau)\cos\Delta\omega\tau+y(\tau)\sin\Delta\omega\tau]d\tau. \tag{32}$$

Since the pulsed double-resonance experiment samples the real part of the decay function, Fourier transformation of this signal alone will always give a line shape symmetrical about ω_{0S}. To observe asymmetry, it is necessary to map out the FID with the S-channel rf off resonance by an amount Ω, greater than the largest shift δ_i. The absorption line shape produced is then

$$\Gamma''(\Delta\omega)=K\sum_i a_i[\delta(\Delta\omega+\delta_i+\Omega)+\delta(\Delta\omega-\delta_i-\Omega)]. \tag{33}$$

This expression, though still symmetric about ω_{0S}, can be asymmetric about $\omega_{0S} \pm \Omega$. Provided the sign of the resonance offset, Ω, is known, the correct side of the doublet, Eq. (33) may be selected. Inclusion of the neglected $y(\tau)$ would perform this selection automatically.

D. Analogue-Fourier-Transform Spectroscopy

1. Variable Off Time

In Sec. II B 3 the destruction spectrum modulation effect discussed there was not the S-spin line shape. In fact it is easy to see from Eqs. (20) and (21) that what is observed is just the logarithm of one Fourier component of the line shape. A superposition of many such single spectra, produced from a series of separate experiments for various values of τ, could in principle generate the true S-spin line-shape function. However, as we shall show in this section, the whole Fourier spectrum may be sampled in a single experiment by varying the off time following consecutive thermal mixing pulses. This in turn allows the S-spin line shape to be determined within a single frequency sweep.

We ask what is the ratio of final-to-initial I magnetization in response to N thermal contacts of duration t and variable off time τ_n. A simple generalization of our previous formula [Eq. (11)] gives for the new matrix equation

$$\begin{pmatrix} M_{IN} \\ M_{SN}/\eta \end{pmatrix} = T \prod_{i}^{N} \underline{A}(\tau_n) \begin{pmatrix} 1 \\ 0 \end{pmatrix} M_{0I} \ , \tag{34}$$

where T is a time-ordering operator which orders the times τ_n in descending (or ascending) rank from left to right. The matrix $\underline{A}(\tau_n)$ is as defined previously, Eq. (10), and does not commute with itself for different times. In order to obtain M_{IN}, we adopt the following approach: Let the unitary matrix which diagonalizes $\underline{A}(\tau_n)$ be $\underline{S}(\tau_n)$; then

$$\underline{S}^{\dagger}(\tau_n)\,\underline{A}(\tau_n)\,\underline{S}(\tau_n) = \underline{\Lambda} \ . \tag{35}$$

The eigenvalues of $\underline{\Lambda}$ are found to be $\lambda_{11}(\tau_n) = k_+$ and $\lambda_{22}(\tau_n) = k_-$. The matrix elements of $\underline{S}$ are found to be

$$\begin{aligned} &S_{11} = 1 , \qquad S_{12} = d/(c - k_+) , \\ &S_{21} = -S_{12} , \quad S_{22} = -d^2/(c - k_+)(c - k_-) . \end{aligned} \tag{36}$$

The longest time τ_N is chosen to make $\tau_N \gg T_{2S}$, so that $\Gamma(\tau_N) = 0$. In order to span the rare-spin FID uniformly, we choose $\tau_n = n\tau_{0S}$, n an integer. Rearrangement of Eq. (35) above and substitution in Eq. (34) yields in the limit $\tau_{0S} \to 0$ with $\tau_N = N\tau_{0S}$ held constant and with the given incremental ordering

$$\begin{pmatrix} M_{IN} \\ M_{SN}/\eta \end{pmatrix} = \underline{S}(\tau_N) \prod_{1}^{N} \underline{\Lambda}(\tau_n)\,\underline{S}^{\dagger}(\tau_1) \begin{pmatrix} 1 \\ 0 \end{pmatrix} M_{0I} . \tag{37}$$

Since $\underline{\Lambda}(\tau_n)$ is diagonal, the time ordering of this product is no longer important in mathematical manipulations. However, the ordering of the $\underline{S}$ operators is important. That is to say, it makes a difference whether the experiment is arranged to proceed with ascending or descending rank of τ_n. We shall see later on that this could be an important consideration if many cycles of a particular sequence are required.

Evaluating Eq. (37), we find for the magnetization component

$$M_{IN}/M_{0I} = [S_{11}(\tau_N) S_{22}(\tau_1) \prod_{1}^{N} k_+(\tau_n) - S_{12}(\tau_N) S_{21}(\tau_1) \prod_{1}^{N} k_-(\tau_n)]/\det \underline{S}(\tau_1) . \tag{38}$$

2. Approximations

As for the case with constant τ, we specialize to the situation $\Gamma(\tau_n) e^{-t/T_{CR}} = 0$; that is $t \gg T_{CR}$. Equation (38) becomes for descending n

$$\frac{M_{IN}}{M_{0I}} = a \prod_{2}^{N} k_+(\tau_n) \tag{39a}$$

and for ascending n

$$\frac{M_{IN}}{M_{0I}} = a \prod_{1}^{N-1} k_+(\tau_n) . \tag{39b}$$

If we now generalize our result by considering the response to N thermal contacts comprising M cycles of L spin-mixing pulses plus one, of duration t, and variable off time τ_{ml} we get, instead of Eq. (39b),

$$\frac{M_{IN}}{M_{0I}} = a \prod_{1}^{M} \prod_{1}^{L} k_+(\tau_{ml}) , \tag{40}$$

where $N = LM + 1$ since both initiating and terminating thermal mixing pulses are required. As a consequence of the ordering operator, the sequence of S pulses starts with long τ_{1L} and whistles up to short τ_{11}. Subsequent cycles each follow in *reflection symmetry* to the previous cycle.

Substitution of a and k_+ from Eqs. (10) and (15) into Eq. (40) gives for $\epsilon \ll 1$,

$$\frac{M(N)}{M(0)} = (1 + \epsilon)^{-1} \exp\left(-\sum_{1}^{M} \sum_{1}^{L} \epsilon[1 - \Gamma(\tau_{ml})] \right) . \tag{41}$$

If the rare-spin FID is spanned uniformly during each cycle and $\Gamma(\tau_{mL}) = 0$, the summation in Eq.

(41) performs the analogue Fourier transform of the FID. For M identical cycles we may write Eq. (41) as

$$\frac{M(N,\Delta\omega)}{M(0)} = (1+\epsilon)^{-1}\exp\{-[(N-1)\epsilon - M\epsilon\Gamma''(\Delta\omega)]\}, \quad (42)$$

where $\Gamma''(\Delta\omega)$ is the real part of the complex susceptibility; that is

$$\Gamma''(\Delta\omega) = \sum_{1}^{L}\Gamma(\tau_I). \quad (43)$$

This follows directly from trigonometric expansion of $\Gamma(\tau)$. The amplitude of $\Gamma''(\Delta\omega)$ at resonance may be estimated from Eq. (43), assuming a Gaussian-decay function, in which case $\Gamma''(0) \simeq \frac{1}{2}L$.

A schematic diagram of the pulse sequence just described is shown in Fig. 1, in this case for a single cycle and with the time ordering descending in rank (decreasing in interval) from left to right.

III. SIMULATED EXPERIMENTS

In the previous section a number of approximations were necessary in order to reduce the exact expression for magnetization $M(N)$ to simple and usable forms. In this section we wish to examine the range of validity of the expressions derived by relaxing the inequalities somewhat. In all cases the regenerated decay or line-shape function produced in the simulated double-resonance experiment is compared with the original analogue function.

A. Decay Function

Equation (17) has been evaluated exactly for the simulated Gaussian input function $\Gamma(\tau) = e^{-a^2\tau^2/2}$ in Eqs. (10b)–(10e). The approximate equation

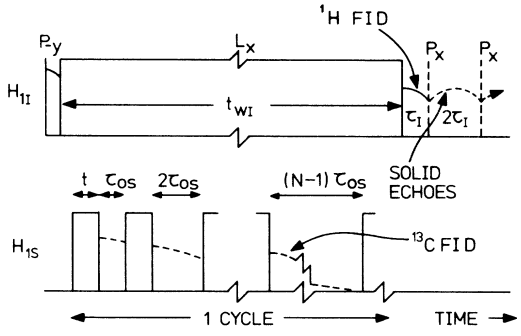

FIG. 1. Sketch of the rf pulse sequences used for double-resonance analogue-Fourier-transform spectroscopy. The FID following the I spin-locking pulse may be lengthened by a multipulse (Ref. 55) sequence $(\tau_I - P_x - \tau_I)_n$, shown in broken lines, for multiple sampling and signal-to-noise enhancement. The S-spin FID, drawn in broken lines, between the S pulses is not observed directly in our experiment.

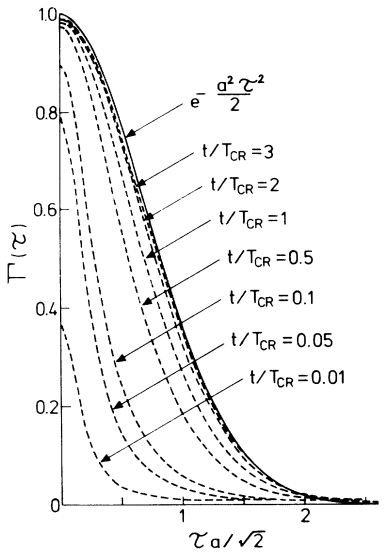

FIG. 2. Theoretical behavior of the regenerated decay function vs τ in a FID mapping experiment, Eq. (44). Decrease of the parameter t/T_{CR} causes the predicted decay function to depart from the ideal result corresponding to the Gaussian input function. In all cases, $N=100$ and $\epsilon = 5.54\times10^{-3}$. The curve $t/T_{CR}=2$ corresponds approximately to the condition used in the PTFE experiments (see Fig. 10).

used to regenerate this function is Eq. (20). Neglecting $\epsilon\Gamma(\tau)$ and rearranging this gives

$$\Gamma(\tau) = \ln[M(N)/M(0)]/N\epsilon + 1 + e^{-t/T_{CR}}. \quad (44)$$

This equation has been evaluated for various values of $a\tau/\sqrt{2}$ and the parameters ϵ, N, t/T_{CR}.

1. Basic Test

If the approximations are satisfied, i.e., $\epsilon \ll 1$ and $t/T_{CR} \gg 1$, then, of course, we expect $\Gamma(\tau) \to e^{-a^2\tau^2/2}$ in Eq. (44). For $\epsilon = 10^{-3}$, $N=100$, and $t/T_{CR} = 100$, the Gaussian is regenerated to better than 0.5% of the maximum normalized amplitude.

2. The Inequality $t/T_{CR} \gg 1$

The simulated decay was calculated for $\epsilon = 5.54\times10^{-3}$ and $N = 100$ for various values of the ratio t/T_{CR}. These results are plotted in Fig. 2. For $t/T_{CR} < 1$ the regenerated decay shape is seen to have substantial distortion as well as a marked reduction in dynamic range. For $t/T_{CR} = 2$ the maximum error is ~3%. This error reduces to ~1.5% for $t/T_{CR} = 3$.

3. Variation of N

The simulated decay was calculated for various values of N for $t/T_{CR} = 3$ and $\epsilon = 0.01$ and 0.001.

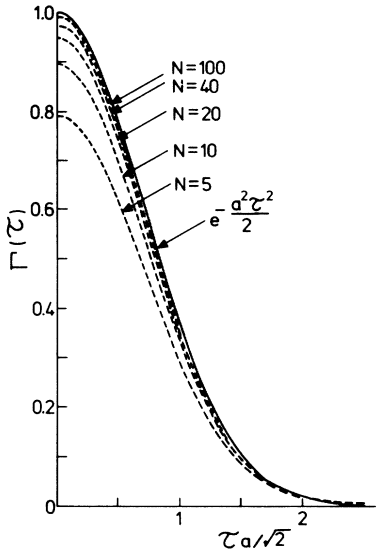

FIG. 3. Theoretical behavior, Eq. (44) of the regenerated decay function $\Gamma(\tau)$ vs τ for variation of the number of thermal contacts N. The rescaled shape functions agree quite well with the Gaussian input function. For all curves the fixed parameters are $\epsilon = 0.01$ and $t/T_{CR} = 3$.

Figure 3 shows the data for $\epsilon = 0.01$. No noticeable change was observed for $\epsilon = 0.001$. It is seen that for $N \geq 100$ and $\epsilon = 0.01$ to 0.001 (the likely limits for ^{13}C in natural abundance) the error is $\sim 1.0\%$. For smaller N it seems that the shape function remains good, but scaled in amplitude. Thus, as expected, the regenerated shape function is substantially independent of N.

B. Regenerated Analogue Line Shape

The normalized regenerated line shape

$$\Gamma'_A = \Gamma''(\Delta\omega)/\Gamma''(0) \tag{45}$$

has been evaluated using $\Gamma''(\Delta\omega)$ from the rearranged equation (42): that is,

$$\Gamma''(\Delta\omega) = \{\ln[M(N)/M(0)] + \ln(1+\epsilon)\}/M\epsilon + L\,. \tag{46}$$

The magnetization $M(N)/M(0)$ is evaluated exactly from the matrix equation (34). This particular normalization procedure tests the form and detailed appearance of M, ϵ, and L in Eq. (46). Clearly this equation has been derived under certain conditions and in the last section was shown to hold when these conditions were met. If we now purposely violate these conditions, the exact functional dependence of $\Gamma''(\Delta\omega)$ on M, ϵ, and L will become more critical in such matters as normalization, for example.

The input function in this case is taken to be

$$\Gamma(\tau) = e^{-a^2\tau^2/2}\cos\Delta\omega\tau\,. \tag{47}$$

Equation (46) was evaluated for various values of the parameters ϵ, L, M and for each set of parameters a parametric family of graphs was produced varying t/T_{CR}. A representative example of such a result is shown in Fig. 4. The results are compared with the theoretical Gaussian line shape $\exp[-(\Delta\omega^2/2a^2)]$ and in all cases, the data flatten off to a nonzero base line, the height of which increases with decreasing ratio t/T_{CR}. In fact, as seen, the fit for $M = 2$, $t/T_{CR} = 100$, and $L = 100$ in Fig. (4) is quite good. However, for $L < 60$ and $t/T_{CR} = 100$, increasing M can cause the base line to go slightly negative, a clearly unphysical situation.

The most important factor in the regenerated line is the shape itself. The large variation in dynamic range with change of t/T_{CR} prevents easy comparison. By defining a different normalization procedure, the shapes may be compared directly. An alternative normalization procedure is defined as follows:

$$\Gamma''_B(\Delta\omega) = \frac{\Gamma''(\Delta\omega) - \Gamma''(\Omega)}{\Gamma''(0) - \Gamma''(\Omega)}\,, \tag{48a}$$

where Ω is chosen to be well away from the line

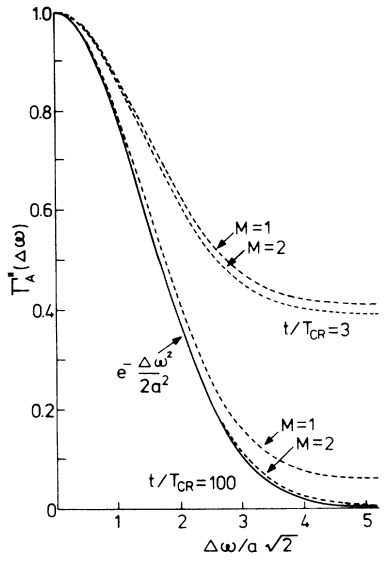

FIG. 4. Theoretical behavior of the regenerated normalized line shape $\Gamma''_A(\Delta\omega)$ vs $\Delta\omega$ in a double-resonance analogue-Fourier-transform experiment, Eqs. (45) and (46). Quite large variations of the base line are produced as the cross-relaxation parameter t/T_{CR} is varied. Also shown is the effect of two identical cycles of thermal mixing pulses ($M = 2$ unsymmetrized). The Gaussian input function is also given for comparison. In all cases, $\epsilon = 10^{-2}$, $L = 100$, $M = 1$, and $\tau'_{0S} = \tau_{0S}/T_{2S} = 0.10$.

center, on the angular frequency-independent plateau. Substituting Eq. (46) into Eq. (48a), we obtain the following form:

$$\Gamma''_B(\Delta\omega)=\frac{\ln[M(N,\Delta\omega)/M(N,\Omega)]}{\ln[M(N,0)/M(N,\Omega)]}\ , \qquad (48b)$$

which is independent of the particular functional dependence on ϵ, M and L implicit in Eq. (46). This is clearly a more fundamental test of the whole process of line-shape regeneration by the analogue-Fourier-transform method, since no approximation need be made and $M(N, \Delta\omega)/M(0)$ is evaluated exactly directly from Eq. (34).

Using this normalization procedure with $\Omega/\sqrt{2}a = 5.2$, the simulated shape functions for $\epsilon = 10^{-2}$, $L = 10$, $t/T_{CR} = 100$, and $M = 1, 2, 3, 4, 5$ all show no distinguishable difference from the theoretical Gaussian curve. For small values of the ratio t/T_{CR} slight variation of the shape function is observed (Fig. 5).

It is concluded that incomplete cross relaxation mainly shrinks the dynamic range $\Gamma''(0)-\Gamma''(\Omega)$ and causes only slight distortion of the line shape, that is, approximately 4.0% for $t/T_{CR} \sim 0.5$, and less than 1.0% for $t/T_{CR} = 3$.

1. *Truncation Errors*

If the number of sampling points L of the decay is too small so that the FID is not completely

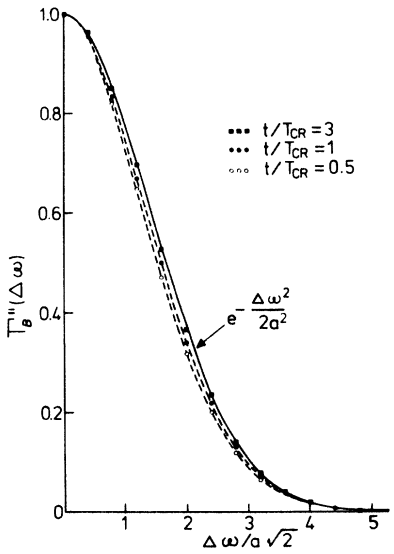

FIG. 5. Theoretical behavior of the regenerated normalized line shape $\Gamma''_B(\Delta\omega)$ vs $\Delta\omega$ in a double-resonance analogue-Fourier-transform experiment, Eq. (44), but using the normalization procedure of Eq. (48). For $t/T_{CR} = 3$ no significant departure from the Gaussian input function is predicted. For all curves $\epsilon = 10^{-2}$, $L = 50$, $M = 2$ (unsymmetrized), and $\tau'_{0S} = \tau_{0S}/T_{2S} = 0.20$.

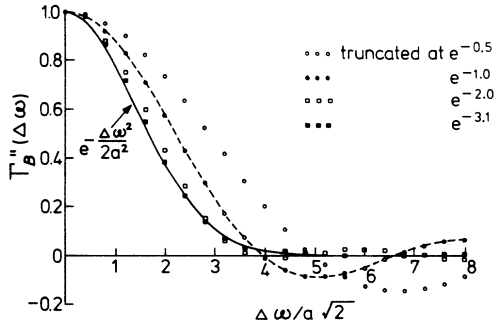

FIG. 6. Effect of decay-sampling truncation on the regenerated line shape in an analogue transform experiment. Equations (44) and (48) are plotted for a truncated Gaussian input decay function, with variation of the truncation point (through variation of τ_{0S}). The results are compared with the computed Fourier transform of the Gaussian input and truncated Gaussian input functions. In all cases $\epsilon = 10^{-3}$, $L = 50$, $M = 2$ (unsymmetrized), and $t/T_{CR} = 100$.

spanned, one expects truncation errors in normal Fourier transforms. That these occur in the analogue-transform method is demonstrated in Fig. 6. Here the truncation is achieved at constant L by reducing the time interval τ_{0S}. The simulated truncation is compared with the computed Fourier transform corresponding to $\tau'_{0S} = \tau_{0S}/T_{2S} = 0.02$, giving excellent agreement.

In setting up double-resonance analogue-Fourier-transform experiments one should, of course, choose τ_{0S} such that $2\pi/\tau_{0S}$ is much greater than the largest frequency of interest, in order to avoid Fourier sidebands.

In Fig. 7 conditions are simulated corresponding to those used to study ^{13}C in adamantane (discussed in Sec. IV). The presence of a small beat is seen which corresponds to a truncation error and is more pronounced for increasing t/T_{CR}. The curve is compared with the Gaussian function.

2. *Dynamic Range*

The true dynamic range $\ln[M(N, 0)/M(N, \Omega)]$ varies in a complicated way with variation of t/T_{CR}. No expression simpler than the exact expression or Eq. (39) has been derived to describe this variation.

IV. COMPARISON OF SENSITIVITIES

In this section we wish to compare the sensitivity of the analogue-Fourier-transform-spectroscopy method described in Sec. IID with that of the proton-enhanced nuclear-induction-spectroscopy method developed by Pines *et al.*[31] Unlike our method, which detects the dilute spin line shape indirectly through its effect on the abundant spin

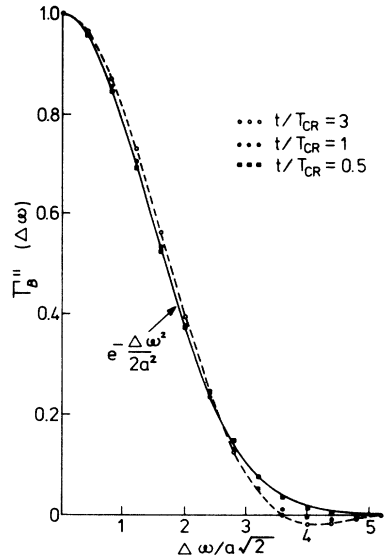

FIG. 7. Effect of varying the cross-relaxation parameter t/T_{CR} on the truncated decay line shape [Eqs. (44) and (48)]. Truncation point corresponds to $\exp(-2.31)$. For $t/T_{CR} \geq 3$ the expected shape is regenerated. For $t/T_{CR} < 3$ the regenerated shape approaches the original Gaussian shape; however, in all cases the deviations are small. For all curves, the fixed parameters were chosen to correspond to those used in the experiments on adamantane: that is, $\epsilon = 6.925 \times 10^{-3}$, $L = 76$, $M = 1$, and $\tau'_{0S} = \tau_{0S}/T_{2S} = 0.02$.

system, the method of Pines *et al.* detects the dilute spins directly and relies on digital averaging to further enhance the signal-to-noise ratio.

A. Sensitivity of Analogue-Fourier-Transform Spectroscopy

It was shown in Sec. II D that in an analogue-Fourier-Transform (F. T.) experiment the I-magnetization destruction changes from $e^{-(N-1)\epsilon}$ to $e^{-(N-1)\epsilon/2}$ as the S-spin line shape is mapped out. Therefore the signal-to-noise ratio R of the absorption line shape given by this indirect method (IND) may be written, for $N \gg 1$,

$$R_{IND} \simeq (e^{-N\epsilon/2} - e^{-N\epsilon}) R_I , \tag{49}$$

where R_I is the signal-to-noise ratio of the I-spin free induction decay.

B. Sensitivity of Proton-Enhanced Nuclear-Induction Spectroscopy

In the Lurie-Slichter double-resonance method, the thermal equilibrium S magnetization resulting from one thermal contact with the polarized I spins is

$$M_{Sf} = \frac{C_S H_0}{\Theta_L} \left(\frac{H_{1I}}{H_{1S}}\right) \frac{1}{1+\epsilon} . \tag{50}$$

From Eq. (3), the Curie law, it is evident that $C_S H_0/\Theta_L$ is the amplitude of the intrinsic S-spin free-induction decay. Therefore, if the Hahn condition $\omega_{1I} = \omega_{1S}$ is satisfied, one thermal contact enhances the S nuclear signal by a factor $(\gamma_I/\gamma_S)(1+\epsilon)$. If the S nuclear signal is stored electronically, then after N thermal contacts in one pulse train the enhanced signal-to-noise ratio of the direct (DIR) method is

$$R_{DIR} = R_S \frac{\gamma_I}{\gamma_S} N^{-1/2} \sum_{i=1}^{N} (1+\epsilon)^{-i} , \tag{51}$$

where the factor $N^{-1/2}$ arises from the random thermal noise in the receiver. For $\epsilon \ll 1$, Eq. (51) gives

$$R_{DIR} = (\gamma_I/\gamma_S)(\epsilon\sqrt{N})^{-1}(1 - e^{-N\epsilon}) R_S . \tag{52}$$

If $H_{1I} \gg H_L$ so that $\epsilon = N_S/N_I$, and $N\epsilon \gg 1$, Eq. (52) is essentially the result given by Pines *et al.*[31]

C. Relative Sensitivity

The ratio of the initial amplitudes of the intrinsic free-induction decays of the I and the S spins is given by[49]

$$\frac{R_I}{R_S} = \frac{N_I}{N_S} \left(\frac{\gamma_I}{\gamma_S}\right)^3 \frac{I(I+1)}{S(S+1)} \frac{A_I}{A_S} \left(\frac{W_S}{W_I}\right)^{1/2} , \tag{53}$$

where A_I, A_S are the receiver-coil area turns and W_I, W_S are the receiver bandwidths. The inductance of the receiver coil is proportional to the square of the number of turns, so that

$$A_I/A_S \simeq \gamma_S/\gamma_I . \tag{54}$$

The bandwidth required to give the S-spin line shape undistorted is about $10/T_{2S}$. However, in the analogue-F. T.-spectroscopy experiment, the detailed line shape of the I spins is of no interest, so a bandwidth $1/T_{2I}$ will suffice. Therefore

$$(W_S/W_I)^{1/2} \simeq (10 T_{2I}/T_{2S})^{1/2} . \tag{55}$$

Thus Eqs. (49) and (52)–(55) give for the relative sensitivity

$$\frac{R_{IND}}{R_{DIR}} = \frac{\gamma_I}{\gamma_S} \frac{I(I+1)}{S(S+1)} \left(\frac{10\,T_{2I}}{T_{2S}}\right)^{1/2} F\left[\frac{e^{-N\epsilon/2} - e^{-N\epsilon}}{1 - e^{-N\epsilon}}\right]\sqrt{N}, \tag{56}$$

where F is an enhancement factor introduced to take account of single shot averaging of the I magnetization in the indirect method (see Sec. VI).

If $N\epsilon \ll 1$, the function in square brackets may be replaced by $\frac{1}{2}$ for all N. In this case the relative sensitivity depends on $\sqrt{N}$ and for ^{13}C and ^{1}H, and taking $T_{2I}/T_{2S} = 10^{-2}$, we find that

$$R_{IND}/R_{DIR} \simeq \tfrac{2}{3} F\sqrt{N} . \tag{57}$$

If we put $N\epsilon = \chi$ in Eq. (56), we obtain an alternative expression for the relative sensitivity:

$$\frac{R_{IND}}{R_{DIR}} = \frac{\gamma_I I(I+1)}{\gamma_S S(S+1)} \left(\frac{10 T_{2I}}{T_{2S}}\right)^{1/2} \frac{F}{\sqrt{\epsilon}} G(\chi), \quad (58)$$

where

$$G(\chi) = \left[\frac{e^{-\chi/2} - e^{-\chi}}{1 - e^{-\chi}}\right] \sqrt{\chi} \ . \quad (59)$$

The function $G(\chi)$ has a maximum of ~ 0.39 when $\chi \simeq 1.5$. Equation (58) emphasizes the dependence of the relative sensitivity on the dilution parameter ϵ.

D. Conclusion

For $\epsilon \sim 10^{-2}$ and $N > 3$, Eq. (57) shows that for $F = 1$ the relative sensitivity may be greater than 1. In the case where the number of pulses is optimized, Eq. (58) shows for $\epsilon = 10^{-2}$ and $F = 1$ that the relative sensitivity is about 5.

The main difficulty with the proton-enhanced technique is that the receiver detecting the S nuclear signal must not be saturated by the I rf field. This is easier to achieve, the higher the static field, so that the frequency difference $\omega_{0I} - \omega_{0S}$ is greater. If very high static fields are available, the sensitivity advantage of the analogue F. T. experiment may be superfluous.

An important advantage of the proton-enhanced method, not accounted for in our calculation of relative sensitivity is that it samples the complete FID of the dilute spin system. Thus, though intrinsically less sensitive, the method acquires data more quickly and is therefore, in principle, less demanding of the over-all equipment stability.

Of course, in order to achieve the *same* signal-to-noise ratio for the direct method as obtained in the indirect method, for the same number of pulses N, the direct-method experiment would have to be repeated ~ $1/\epsilon$ times. If this number is greater than the number of decay sample points L in the indirect method, then the above comment regarding stability no longer applies. Indeed, in this case the total time to acquire the same information is shorter for our indirect method.

V. EXPERIMENTAL RESULTS

In this section we describe a number of experimental results on the 1.108%-abundant ^{13}C in various samples, chosen to illustrate the various predictions of the theory developed in Sec. II.

A. Destruction Spectrum Modulation

A test of the predictions of Eq. (20) was performed on ^{13}C in polytetrafluoroethylene [PTFE, $(C_2F_4)_n$] at 77 °K. The sample was ordinary commercial-grade amorphous material. The observed spins (^{19}F) were spin locked at resonance (15 MHz). For large rf fields satisfying the Hahn condition $\omega_{1I} = \omega_{1S}$ the ratio of the thermal capacities of the two spin systems (both spin-$\frac{1}{2}$) [Eq. (6)], $\epsilon = N_S/N_I$, and in the present case $\epsilon = 5.54 \times 10^{-3}$. Since the carbons are equivalent on the polymer chain, only a single ^{13}C resonance is expected.

Figure 8(a) shows the details of the periodic structure in the destruction spectrum for $\tau < T_{2S}$. For $\tau > T_{2S}$, the same material gave a 50-kHz broad unmodulated line, part of which is superimposed on Fig. 8(a). The linewidth in this case is controlled mainly by the fluorine-fluorine dipolar interaction. The central line in the modulated spectrum is, by contrast, reduced by two orders of magnitude to ~ 600 Hz. The central frequency of this spectrum can be determined unambiguously, since it should not change as τ is varied, at least for a single symmetrical line.

In Fig. 8(b) a detailed study of the central peak is shown for two values of τ. The solid line is

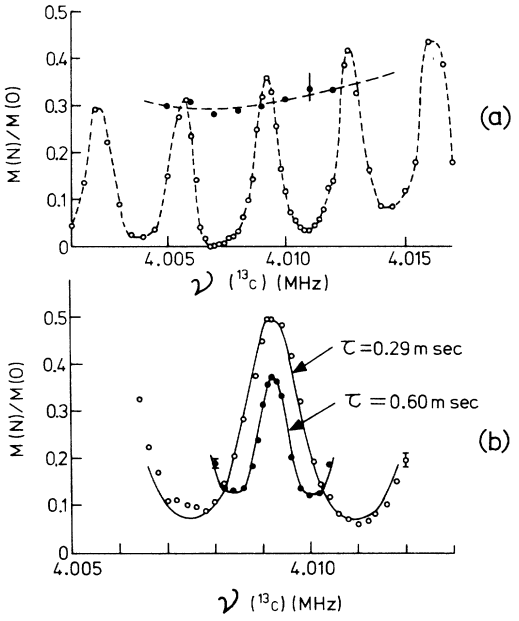

FIG. 8. (a) Normalized ^{19}F destruction spectra in PTFE at 77 °K. The filled circles show a broad unmodulated line which is part of a conventional double-resonance destruction spectrum with $N = 150$, $t = 1.0$ msec, and $\tau = 3.5$ msec. The open circles show clear modulation of the spectrum, as expected from Eqs. (20) and (21). In this case $N = 600$, $t = 0.1$ msec, and $\tau = 0.3$ msec. (b) Detailed study of the central peak of the spectrum as in (a), showing the improved resolution with increasing τ. For the open circles $N = 400$, $t = 0.1$ msec, and $\tau = 0.29$ msec, while for the closed circles $N = 300$, $t = 0.2$ msec, and $\tau = 0.60$ msec. The full curves are Eq. (20) normalized to amplitude only. In both (a) and (b) it is estimated that $T_{2S} \sim 1.0$ msec and $T_{CR} \sim 0.4$ msec. Also $\omega_{1I}/2\pi = \omega_{1S}/2\pi = 19.3$ kHz. In all cases it has been arranged that the Fourier harmonics of the S pulse train fall outside the first destruction minima.

the theoretical expression [Eqs. (20) and (21)] fitted for amplitude only in both cases.

In PTFE the ^{13}C line is broadened slightly by an anisotropic chemical-shift tensor, so the central peak of the modulated destruction spectrum is expected to change slightly according to Eq. (25). The central peak shift has been measured as a function of τ and the results presented in Fig. 9. The data are compared with the theoretical prediction, Eq. (27), in which the third moment is estimated directly from the absorption line shape, details of which are discussed later. We see that the isotropic chemical shift of the spectrum with respect to some external reference can be determined by extrapolating the data in Fig. 9 to zero τ. We have used such a procedure to estimate the effective magnetogyric ratio of ^{13}C in PTFE.[27]

In general, if a spectrum is broadened by an anisotropic chemical-shift tensor, then a plot such as Fig. 9 is some sort of measure of the anisotropy. It is well known that, for a spectrum broadened by an anisotropic chemical-shift tensor with axial symmetry, the second moment, taken about the point which makes the first moment vanish, may be simply expressed in terms of the difference between the parallel $\omega_{\parallel}$ and perpendicular $\omega_{\perp}$ shift components.[43] Unfortunately the third moment taken about the same spectral point is not expressible so simply. Thus measurement of M_3 alone cannot be used to estimate the shift anisotropy. We now turn to more direct measurements of chemical-shift anisotropy.

B. The ^{13}C FID in Polytetrafluoroethylene

The structure and configurational characteristics of PTFE have been reviewed recently by Bates.[44] The PTFE macromolecule is linear and composed of $-CF_2$ units, molecular weights being several millions. The zig-zag skeletal carbons lie on a helix. In the phase below 19 °C, the 180° repeat unit of this helix comprises thirteen CF_2 groups with a repeat distance of 16.8 Å and a C–C–C angle of 116°. In the bulk material both crystalline and amorphous phases co-exist; in the crystalline bands the macromolecules pack like cylindrical rods into an almost hexagonal array.

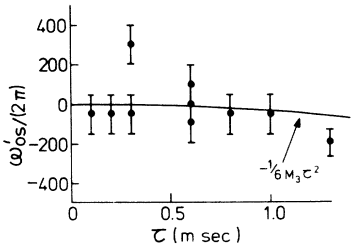

FIG. 9. Variation of the apparent resonance frequency $\omega'_{0S}/2\pi$ (in Hz) of the ^{13}C spins in PTFE at 77 °K for various off times τ determined from amplitude-modulated ^{19}F destruction spectra like those in Fig. 8. The curve is Eq. (27) with M_3 estimated graphically from the experimental points in Fig. 10.

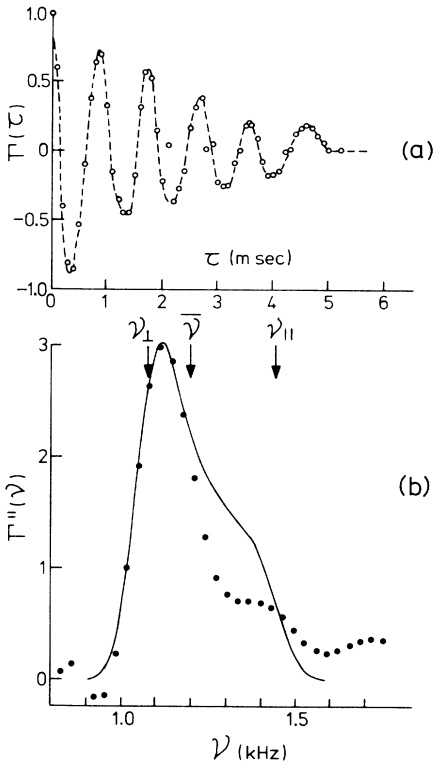

FIG. 10. Fourier-transform spectroscopy of ^{13}C in PTFE at 77 °K. (a) The ^{13}C FID mapped out by the ^{19}F residual magnetization with $N=100$, $t=1.0$ msec, $H_{1I}=6.0$ G, and $\omega_{1I}=\omega_{1S}$. The S-channel rf carrier frequency $\omega_S/2\pi=4.008\,000$ MHz. (b) The points are the Fourier cosine transform of the FID data in (a). Only the high-frequency component of the doublet is given ($\omega_S<\omega_{0S}$). The full curve is the Gaussian-convoluted polycrystalline average chemical-shift line shape, corresponding to an axially symmetric shift tensor with $\bar{\sigma}=-130\pm25$ ppm and the traceless components $\Delta\sigma_{\perp}=-30$ and $\Delta\sigma_{\parallel}=60$ ppm relative to CH_3I (Ref. 45).

The ^{13}C FID in PTFE at 77 °K was obtained by the double-resonance mapping method described in Secs. II A–II C. The ^{19}F spins were spin locked at resonance (~ 15 MHz) in an rf field $H_{1I}=6.0$ G, while the ^{13}C spins were irradiated by a train of $N=100$ equally spaced thermal contact pulses with $t=1.0$ msec, and $\omega_{0S}-\omega_S\sim1$ kHz. The Hahn condition was approximately satisfied. The off time was varied from 0 to 5 msec and the spin-locking pulse was also increased in length. The decay obtained is shown in Fig. 10(a). Each point was separately normalized in the experiment. The dynamic range of the decay data is about 40% of the ^{19}F magnetiza-

tion. The Fourier cosine transform of the decay data is given in Fig. 10(b), and the line shape shows some chemical-shift anisotropy.

The isotropic chemical shift of ^{13}C in PTFE is found to be $\bar{\sigma} = -130 \pm 25$ ppm relative to CH_3I.[45] It was attempted to fit the data with a Gaussian-broadened powder line shape corresponding to an axially symmetric chemical-shift tensor.[46–49] The best fit achieved is shown in Fig. 10(b) for which the traceless tensor components are $\Delta\sigma_\perp = -30$ ppm and $\Delta\sigma_\parallel = 60$ ppm, with a Gaussian half-width of 106 Hz. A consistently poor fit of the experimental data at high frequencies was found in four independent experiments.

The deviation of the experimental line shape from the theoretical prediction is attributed to partial alignment of the polymer macromolecules along the sample axis. This seems plausible, since the sample was an extruded rod.

C. Analogue-Fourier-Transform Studies

1. ^{13}C Doublet Resolution in Adamantane

Adamantane ($C_{10}H_{16}$) is a cagelike globular molecule with tetrahedral symmetry, comprising six CH_2 and four CH groups. The lattice is face-centered cubic. In the plastic phase, -65 to 280 °C, the molecules are known, from the relaxation-time measurements of Resing[50] to undergo isotropic reorientation and diffusion. At 25 °C the jump rates for rotation and diffusion are about 10^{11} sec^{-1} and 10^{-5} sec^{-1}, respectively.[50] The rapid reorientation averages to zero the chemical-shift anisotropy, leaving only the isotropic shift. Kuhlmann *et al.*,[51] in an Overhauser induction experiment on a solution of adamantane, have measured the chemical shift between the ^{13}CH and $^{13}CH_2$ groups as 9.2 ± 0.1 ppm. This measurement was done at 15 MHz. Adamantane is an ideal compound for a pulsed double-resonance experiment in view of the long $T_{1\rho I}$ and the narrow ^{13}C intrinsic linewidth.

A double-resonance analogue-Fourier-transform experiment was performed on approximately 130 mg of powdered adamantane at 25 °C. For this compound $\epsilon = 6.925 \times 10^{-3}$. The protons were spin locked for 1.1 sec at resonance in an rf field of 5.1 G, while the ^{13}C spins were irradiated by one cycle of 77 thermal contact pulses with $t = 4.0$ msec and off-time increment $\tau_{0S} = 0.25$ msec. The Hahn condition was approximately satisfied with $\omega_{1I}/2\pi = 22$ kHz. Our results are presented in Fig. 11 and show the ^{13}C spectrum at about 3.77 MHz in the central portion of the ^1H destruction spectrum. As expected, the ^{13}C absorption line is a doublet. The observed intensity ratio of 2 : 2.6 and the splitting of 36 ± 5 Hz or 9.5 ± 1.3 ppm are in good agreement with the theoretical intensity ratio 2 : 3 and the results of Kuhlmann *et al.*[51] for a solution and those of Pines *et al.*[31] performed at 22.44 MHz on the solid. The residual linewidth is 20 Hz for the $^{13}CH_2$ component and 30 Hz for the ^{13}CH contribution, the latter being consistently the broader of the two lines in three independent experiments. However, the signal-to-noise ratio of our data is not high enough to press the point. In each case the widths are limited by static magnetic field inhomogeneity due to magnet and probe plus residual heteronuclear dipolar broadening. The intrinsic dipolar linewidth for such a dilute spin system is expected to be about 5 Hz.[52,53]

Strictly speaking, the absorption line shape is the logarithm of the destruction spectrum. However, because of the small dynamic range of the spectrum on a normalized scale, the logarithmic graph differs little from the linear plot.

2. ^{13}C Chemical Shift in Methyl Urea

An analogue-Fourier-transform experiment was performed on a powdered sample of methyl urea ($CH_3NHCONH_2$) at 77 °K. At this temperature it is expected that all molecular motions, except possibly methyl-group rotation, will be frozen out. The protons were spin locked at resonance for 300 msec with $H_{1I} = 6.7$ G, while the ^{13}C spins were irradiated with $M = 2$ cycles (unsymmetrized) of $L = 50$ thermal contact pulses with on-time $t = 1.0$ msec and off-time increment $\tau_{0S} = 0.08$ msec. The Hahn condition was approximately satisfied with $\omega_{1I}/2\pi = 29$ kHz, so that $\epsilon = 3.69 \times 10^{-3}$.

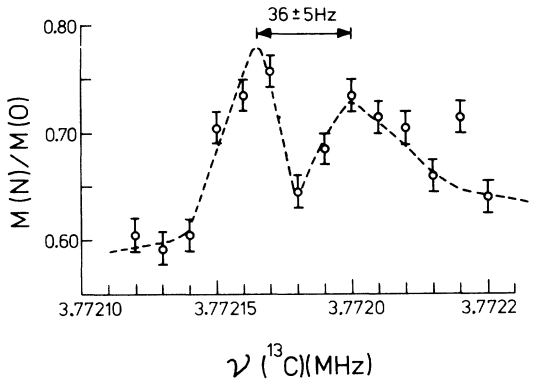

FIG. 11. Normalized ^1H destruction spectrum for solid adamantane ($C_{10}H_{16}$) at 25 °C, showing the absorption line shape of the 1.108%-abundant ^{13}C spins. This was obtained by the analogue-Fourier-transform method described in Sec. II. The experiment reveals a doublet with an intensity ratio 2 : 2.6 and a splitting of 36 ± 5 Hz. This curve was obtained with $M = 1$ cycles of $L = 75$ pulses with $t = 4.0$ msec, $\tau_{0S} = 0.25$ msec, and $\omega_{1I}/2\pi = \omega_{1S}/2\pi = 22$ kHz. Each data point is a ten-count average.

The destruction spectrum is shown in Fig. 12. The ^{13}C absorption spectrum shows two lines, at 3.771 59 and at 3.771 89 MHz. These lines are at -52 ± 8 and -127 ± 8 ppm relative to $^{13}CH_3I$.[45] Without a single crystal orientation study it is difficult to assign these peaks definitely. We can, of course, look to similar chemical groups in other compounds. For example the molecule acetic acid contains both a methyl and carbonyl group for which $\bar{\sigma}(^{13}CH_3-) = -44$ ppm and $\bar{\sigma}(-{}^{13}CO-) = -202$ ppm relative to $^{13}CH_3I$.[54] On this basis we tentatively assign the higher frequency line in our spectrum to the carbonyl site and the other line to the methyl site.

The spectrum signal-to-noise ratio is poor because the intensity corresponding to the fraction ϵ is distributed over a total linewidth of 200 Hz or so and also because the relatively short $T_{1\rho}$ of the protons limited the number N of thermal contacts that could be used.

The carbonyl line exhibits chemical-shift anisotropy. The polycrystalline average line shape convoluted with a Gaussian-broadening function was computed. The tensor components and the Gaussian width were adjusted for best fit of the data. The solid curve in Fig. 12 is the theoretical line shape corresponding to the traceless-tensor-component values $\Delta\sigma_{11} = -17$, $\Delta\sigma_{22} = -5$, and $\Delta\sigma_{33} = 22$ ppm, with $\bar{\sigma} = -127\pm8$ ppm relative to CH_3I. The Gaussian half-width in the convolution integral was 25 Hz. These values must be considered as tentative, since the rather large noise variation on the spectrum scarcely permits a unique determination of the chemical-shift anisotropy.

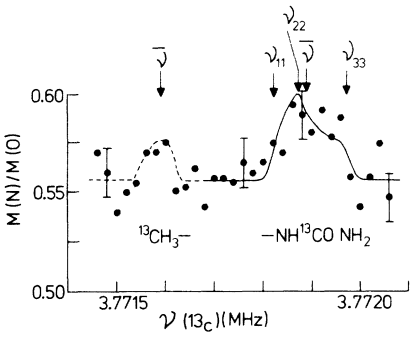

FIG. 12. Normalized ^{1}H destruction spectrum for solid methyl urea ($CH_3NHCONH_2$) at 77 °K obtained by the analogue-Fourier-transform method. The ^{13}C absorption line shape shows two lines, which we tentatively ascribe to the methyl and carbonyl sites in the molecule, as indicated. The carbonyl carbon exhibits chemical-shift anisotropy. The full curve is the theoretical Gaussian convoluted powder average line shape corresponding to the tracless tensor components $\Delta\sigma_{11} = -17$, $\Delta\sigma_{22} = -5$, $\Delta\sigma_{33} = 22$, with $\bar{\sigma} = -127\pm8$ ppm relative to $^{13}CH_3I$ (Ref. 45). These data were obtained with $M = 2$ cycles (unsymmetrized) of $L = 50$ thermal contacts with $t = 1.0$ msec, $\tau_{0S} = 0.08$ msec, and $\omega_{1I}/2\pi = \omega_{1S}/2\pi = 29$ kHz. Each data point is a 20-count average.

The methyl line is puzzling when compared with the carbonyl line: it is much weaker and shows no resolvable chemical-shift structure. At 77 °K it is likely that the methyl group is reorienting about the C–N bond at a rate greater than the linewidth, but this should not affect the anisotropic line shape significantly, since for both static and reorienting situations one expects an axially symmetric chemical-shift tensor. Methyl-group reorientation may be responsible for the weakness of the line, since motion could inhibit the cross relaxation between the methyl carbon and some of the protons, although frankly this seems unlikely in view of the ^{1}H magnetization amplitude which, away from the two lines, is consistent with $t \gg T_{CR}$.

VI. CONCLUSIONS

New variants of the pulse double-resonance technique are proposed which allow the FID and the absorption line shape of a dilute-spin system to be measured in situations where there is a second high-abundance spin species. The theoretical expressions for decay shape and line shape have been evaluated in parametric form on a computer. The results of this evaluation give the range of validity of the technique. Values of the parameters common to ^{13}C studies in many solid organic compounds indicate that ^{13}C line shapes, in particular chemical shifts and shift anisotropies, are in principle measurable by our scheme. Whether or not they are in fact measurable will depend on the spin-lattice relaxation times T_1 and $T_{1\rho}$ of both the abundant and rare-spin species and also the cross-relaxation time T_{CR}. The explicit dependence of line shape, etc. on T_1 and $T_{1\rho}$ has not been given, since we assume throughout that spin-lattice relaxation-time effects may be ignored. Generally speaking we require $T_{1\rho}$ to be as long as possible and T_1 and T_{CR} to be short.

Examples of the application of our method are given for ^{13}C line shapes in PTFE, adamantane, and methyl urea. The measurements for adamantane were performed at 25 °C; all others were made at 77 °K. These preliminary results indicate that the method can be used to measure chemical-shift splittings and chemical-shift anisotropy in solids.

Although the signal-to-noise ratio in our spectra is poor, analysis shows that it compares favorably with other methods if the experiment is performed at the *same* value of the static field. An idea for signal-to-noise ratio improvement so far not exploited in this work is to repeatedly sample the artificially narrowed FID of the abundant spins following turn-off of the spin-locking pulse.

This is achieved by applying a series of coherent 90° rf pulses in the sequence $(\tau_I - 90° - \tau_I)_n$ as depicted schematically in Fig. 1.[28,55] Done this way, the multipulse sequence does not interfere with the double-resonance process. In principle a signal-to-noise enhancement by a factor F (see Sec. IV) of about $(T_{2eI}/T_{2I})^{1/2}$ is possible by this means, where T_{2eI} is the effective-decay time constant of the multipulse echo train and T_{2I} is the I species spin-spin relaxation time. For short pulse spacing τ_I, one expects T_{2eI} to approach the rotating-frame spin-lattice relaxation time $T_{1\rho I}$. In adamantane at room temperature, for example, the enhancement factor F is approximately 100.

ACKNOWLEDGMENTS

We wish to thank Dr. J. L. Carolan for writing the Fourier-transform computer program and Dr. W. S. Hinshaw for writing the powder-line-shape program. One of us (P. K. G.) wishes to thank the Science Research Council for providing a research studentship for part of the work covered here.

---

*Work supported by a Science Research Council Equipment Grant.

†Imperial Chemical Industries Limited Postdoctoral Fellow.

[1]S. R. Hartmann and E. L. Hahn, Phys. Rev. **128**, 2042 (1962).

[2]F. M. Lurie and C. P. Slichter, Phys. Rev. **133**, A1108 (1964).

[3]M. Lee and W. Goldburg, Phys. Rev. **140**, A1261 (1965).

[4]A. G. Redfield, Phys. Rev. **130**, 589 (1963).

[5]A. Hartland, Phys. Lett. **20**, 267 (1966).

[6]M. Satoh, P. R. Spencer, and C. P. Slichter, J. Phys. Soc. Jap. **22**, 666 (1967).

[7]M. Kunitomo, T. Terao, Y. Tsutsumi, and T. Hashi, J. Phys. Soc. Jap. **22**, 945 (1967).

[8]R. E. Slusher and E. L. Hahn, Phys. Rev. **166**, 332 (1968).

[9]Y. Tsutsumi, M. Kunitomo, T. Terao, and T. Hashi, J. Phys. Soc. Jap. **24**, 429 (1968).

[10]G. T. Mallick and R. T. Schumacher, Phys. Rev. **166**, 350 (1968).

[11]A. Hartland, Proc. R. Soc. A **304**, 361 (1968).

[12]Y. Tsutsumi, M. Kunitomo, T. Terao, and T. Hashi, J. Phys. Soc. Jap. **26**, 16 (1969).

[13]A. Hartland, J. Phys. C **2**, 264 (1969).

[14]K. F. Nelson and W. D. Ohlsen, Phys. Rev. **180**, 366 (1969).

[15]M. Minier, Phys. Rev. **182**, 437 (1969).

[16]M. Kunitomo, T. Terao, and T. Hashi, Phys. Lett. A **31**, 14 (1970).

[17]M. Schwab and E. L. Hahn, J. Chem. Phys. **52**, 3152 (1970).

[18]D. Stehlik and P. E. Nordal, in *Proceedings of the Sixteenth Congress Ampere, Bucharest,* edited by I. Ursu (North-Holland, Amsterdam, 1970), p. 356.

[19]R. Blinc, M. Mali, R. Osredkar, A. Prelesnik, and I. Zupančić, Chem. Phys. Lett. 9, 85 (1971).

[20]E. P. Jones and S. R. Hartmann, Phys. Rev. B **6**, 757 (1972).

[21]Y. Tsutsumi, M. Kunitomo, and T. Hashi, J. Phys. Soc. Jap. **20**, 2095 (1965).

[22]D. V. Lang and P. R. Moran, Phys. Rev. B **1**, 53 (1970).

[23]P. R. Spencer, H. D. Schmid, and C. P. Slichter, Phys. Rev. B **1**, 2989 (1970).

[24]P. R. Moran and D. V. Lang, Phys. Rev. B **2**, 2360 (1970).

[25]P. Mansfield and G. P. Cant, Phys. Lett. A **33**, 130 (1970).

[26]M. Kunitomo, J. Phys. Soc. Jap. **30**, 1059 (1971).

[27]P. Mansfield and P. K. Grannell, J. Phys. C **4**, L197 (1971).

[28]P. Mansfield and P. K. Grannell, J. Phys. C **5**, L226 (1972).

[29]H. E. Bleich and A. G. Redfield, J. Chem. Phys. **55**, 5405 (1971).

[30](a) C. S. Yannoni and H. E. Bleich, J. Chem. Phys. 55, 5406 (1971); (b) C. S. Yannoni, J. Chem. Phys. 58, 1773 (1973).

[31]A. Pines, M. G. Gibby, and J. S. Waugh, J. Chem. Phys. **56**, 1776 (1972); J. Chem. Phys. 59, 569 (1973).

[32]A. Pines, M. G. Gibby, and J. S. Waugh, Chem. Phys. Lett. **15**, 373 (1972).

[33]M. G. Gibby, R. G. Griffin, A. Pines, and J. S. Waugh, Chem. Phys. Lett. **17**, 80 (1972).

[34]M. G. Gibby, A. Pines, and J. S. Waugh, J. Am. Chem. Soc. **94**, 6231 (1972).

[35]M. G. Gibby, A. Pines, and J. S. Waugh Chem. Phys. Lett. 16, 296 (1972).

[36]L. R. Sarles and R. M. Cotts, Phys. Rev. **111**, 853 (1958).

[37]D. A. McArthur, E. L. Hahn, and R. E. Walstedt, Phys. Rev. **188**, 609 (1969).

[38]M. A. B. Whitaker and P. Mansfield (unpublished).

[39]J. J. Van Vleck, Phys. Rev. **74**, 1168 (1948).

[40]I. J. Lowe and R. E. Norberg, Phys. Rev. **107**, 46 (1957).

[41]C. P. Slichter, *Principles of Magnetic Resonance* (Harper and Row, New York, 1963).

[42]P. Mansfield, Phys. Rev. **151**, 199 (1966).

[43]E. R. Andrew and D. P. Tunstall, Proc. Phys. Soc. Lond. **81**, 986 (1963).

[44]T. W. Bates, in *Fluoropolymers*, edited by L. A. Wall (Wiley, New York, 1972), Vol. 25, p. 451.

[45]A Method for indirect referencing to ^{13}C in methyl iodide was used based on the measurement of the effective magnetogyric ratio. A proton magnetometer was used to measure the frequencies ν_H and ν_I corresponding to resonance of the protons in a water sample and the I spins in the sample, respectively, at the constant spectrometer frequency 14.999 08 MHz. The effective magnetogyric ratio is $(\gamma/2\pi)_{\text{eff}} = (\gamma/2\pi)_{(^1H_2O)}\nu_H/\nu_I$. The magnetogyric ratio of protons in water $(\gamma/2\pi)_{(^1H_2O)}$ has been accurately measured by P. Vigoureux [Nature 198, 1188 (1963)]. For direct comparison with $^{13}CH_3I$ we have taken $(\gamma/2\pi)_{(^{13}CH_3I)} = 1.070\,542 \pm 0.000\,006$ kHz/G. This comes indirectly from V. Royden [Phys. Rev. 96, 543 (1954)], who has measured the frequency ratio $\nu_{(^{13}CH_3I)}/\nu_{(C^1H_3I)}$ and also from taking the relative chemical shift between protons in methyl iodide and water as 2.0 ppm (see Ref. 54, p. 667). The uncertainty in the isotropic shifts is much greater by the indirect method than is customary when using a direct liquid reference. However, the uncertainty in the traceless anisotropic shift components is unaffected.

[46]N. Bloembergen and T. J. Rowland, Acta Metall. **1**, 731 (1953).

[47]N. Bloembergen and T. J. Rowland, Phys. Rev. **97**, 1679 (1955).

[48]P. Mansfield, M. J. Orchard, D. C. Stalker, and K. H. B. Richards, Phys. Rev. B **7**, 90 (1973).

[49]A. Abragam, *The Principles of Nuclear Magnetism* (Claredon, Oxford, England, 1961).

[50]H. A. Resing, Mol. Cryst. Liq. Cryst. **9**, 101 (1969).

[51]K. F. Kuhlmann, D. M. Grant, and R. K. Harris, J. Chem.

Phys. **52**, 3439 (1970).
[52]P. C. Lanterbur, Phys. Rev. Lett. **1**, 343 (1958).
[53]C. Kittel and E. Abrahams, Phys. Rev. **90**, 238 (1953).
[54]J. W. Emsley, J. Feeney, and L. H. Sutcliffe, *High Resolution Nuclear Magnetic Resonance Spectroscopy* (Pergamon, Oxford, England, 1966), Vols. 1 and 2.
[55]For a review of various pulse techniques, including the sequence mentioned here, see, for example, P. Mansfield, in *Progress in Nuclear Magnetic Resonance Spectroscopy*, edited by J. W. Emsley, J. Feeney, and L. H. Sutcliffe (Pergamon, Oxford, England, 1971), Vol. 8, p. 41.